An a posteriori error indicator for discontinuous Galerkin approximations of fourth order elliptic problems

Emmanuil H. Georgoulis*, Paul Houston† and Juha Virtanen‡

June 5, 2008

Abstract

We introduce a residual-based a posteriori error indicator for discontinuous Galerkin discretizations of the biharmonic equation with essential boundary conditions. We show that the indicator is both reliable and efficient with respect to the approximation error measured in terms of a natural energy norm, under minimal regularity assumptions. We validate the performance of the indicator within an adaptive mesh refinement procedure and show its asymptotic exactness for a range of test problems.

1 Introduction

Fourth order boundary-value problems arise in, among other disciplines, thin plate theories of elasticity, phase-field modelling and mathematical biology. For isotropic elastic behaviour of thin plates and membranes, popular models involve the biharmonic operator together with appropriate Dirichlet and Neumann boundary conditions. Finite element methods (FEMs) have proven extremely popular for the numerical treatment of such fourth order elliptic problems. Various finite element methods have been proposed and tested for these problems: from conforming methods in the 1960s (Argyris elements), to non-conforming and mixed FEMs proposed from the 1970s until recently (see, e.g., [8, 12, 14, 6] and the references therein).

Conforming FEMs for fourth order problems require that the finite element space is a finite dimensional subspace of the Sobolev space $H^2(\Omega)$, where Ω denotes the computational domain. To satisfy this conformity requirement, C^1-conforming elements have been, traditionally, introduced (see [10] and the references therein). The implementation of such finite element spaces is highly non-trivial, especially when high order basis functions are involved, or when Ω is a three-dimensional domain; consequently, they are rarely used in practice. Another approach frequently employed in the literature is to rewrite the fourth order problem as a system of second-order problems and use mixed finite element methods (see [8] and the references therein). Additionally, non-conforming FEMs have also been proposed for fourth order problems, cf. [10, 12] for a discussion of the classical (inconsistent) approaches, and the more recent works [14, 7], where C^0-elements are employed on consistent non-conforming discretizations.

*Department of Mathematics, University of Leicester, University Road, Leicester LE1 7RH, United Kingdom. E-mail: Emmanuil.Georgoulis@mcs.le.ac.uk

†School of Mathematical Sciences, University of Nottingham, University Park, Nottingham, NG7 2RD, United Kingdom. E-mail: Paul.Houston@nottingham.ac.uk

‡Department of Mathematics, University of Leicester, University Road, Leicester LE1 7RH, United Kingdom. E-mail: jmv8@le.ac.uk

In recent years, discontinuous Galerkin (DG) finite element methods, a certain class of non-conforming methods, have been receiving considerable attention as flexible and efficient discretizations for a large class of problems ranging from computational fluid dynamics to computational mechanics and electromagnetic theory; see, e.g., [11, 2] and the references therein. The first "modern" DG method for elliptic problems was presented in [3] (which included a formulation for fourth order boundary-value problems as a special case). Recently *hp*-version interior penalty DG finite element methods for the biharmonic problem have been derived in [22, 25, 23, 17], where the stability and a priori error bounds are presented in various settings. The above interior penalty methods are based on the "divergence formulation". Also, [14, 18, 7] and in the recent work [16] on DG methods for the Cahn-Hilliard problem, are concerned with the a priori analysis of interior penalty-type methods for fourth order problems employing "plate formulations".

A posteriori bounds for finite element approximations of fourth order problems in primal formulation have been considered in a number of different contexts: [26, 24] treated the case of C^1-conforming elements; the recent work [5] derived a posteriori bounds for classical non-conforming methods using the Morley element; and [19] developed reliable a posteriori bounds for a C^0-interior penalty method for Kirchoff-Love plates, based on employing Helmholtz decompositions of the error.

The purpose of this work is to present energy norm reliable and efficient a posteriori bounds for the interior penalty discontinuous Galerkin method (IPDG) presented in [25] for the biharmonic problem with essential boundary conditions, under minimal regularity assumptions on the analytical solution. We remark, however, that with minor modifications only, the reliability a posteriori bounds presented here are also applicable to the case of other DG methods for fourth order problems (such as the interior penalty variants presented in [3, 22]) and to the case of various non-conforming methods with C^0-elements, such as the ones presented in [14, 7, 16, 19].

The reliability bound is based on a a suitable recovery operator, which maps discontinuous finite element spaces to H^2_0-conforming finite element spaces (of two polynomial degrees higher), consisting of triangular or quadrilateral macro-elements defined in [13] (cf. also [7, 21, 20] for similar constructions). Using this recovery operator, in conjunction with the inconsistent formulation for the IPDG presented in [17] (which ensures that the weak formulation of the problem is defined under minimal regularity assumptions on the analytical solution), we derive efficient and reliable a posteriori estimates of residual type for the IPDG method in the corresponding energy norm. Some ideas from a posteriori analyses for the Poisson problem presented in [4, 21, 20, 1, 9] are also implicitly utilized here in the context of fourth order problems.

The paper is structured as follows. In Section 2, we present the model problem considered in this work along with the function space framework and the corresponding finite element spaces. In Section 3, we define the suitable recovery operators and prove a suitable bound on the recovery error. The energy-norm reliability and efficiency a posteriori bounds are shown in Section 4, followed by numerical experiments demonstrating their practical performance in Section 5.

2 Preliminaries

We denote by $L^p(\omega)$, $1 \leq p \leq \infty$, the standard Lebesgue spaces, $\omega \subset \mathbb{R}^2$, with corresponding norms $\|\cdot\|_{L^p(\omega)}$; the norm of $L^2(\omega)$ will be denoted by $\|\cdot\|_\omega$ for brevity. We also denote by

$H^s(\omega)$, the standard Hilbertian Sobolev space of index $s \geq 0$ of real-valued functions defined on $\omega \subset \mathbb{R}^2$, along with the corresponding norm and seminorm $\|\cdot\|_{s,\omega}$ and $|\cdot|_{s,\omega}$, respectively.

2.1 Model problem

Let Ω be a bounded open polygonal domain in $\mathbb{R}^2$, and let Γ_∂ denote its boundary. We consider the fourth order equation

$$\Delta^2 u = f \quad \text{in } \Omega, \tag{1}$$

where $f \in L^2(\Omega)$. For simplicity of the presentation, we impose homogeneous essential boundary conditions

$$\begin{aligned} u &= 0 \quad \text{on } \Gamma_\partial, \\ \nabla u \cdot \mathbf{n} &= 0 \quad \text{on } \Gamma_\partial, \end{aligned} \tag{2}$$

where $\mathbf{n}$ denotes the unit outward normal vector to Γ_∂. The case of non-homogeneous boundary conditions may be treated analogously.

2.2 Meshes, finite element spaces and trace operators

Let $\mathcal{T}$ be a conforming subdivision of Ω into disjoint triangular or quadrilateral elements $\kappa \in \mathcal{T}$. We define $h_\kappa := \text{diam}(\kappa)$ and we collect them into the element-wise constant function $\mathbf{h} : \Omega \to \mathbb{R}$, with $\mathbf{h}|_\kappa = h_\kappa$, $\kappa \in \mathcal{T}$. We assume that the subdivision $\mathcal{T}$ is shape-regular (see, e.g., p.124 in [10]) and that it is constructed via affine element mappings F_κ, where $F_\kappa : \hat{\kappa} \to \kappa$, with non-singular Jacobian, where $\hat{\kappa}$ is the reference triangle or quadrilateral. The above mappings are assumed to be constructed so as to ensure $\bar{\Omega} = \cup_{\kappa \in \mathcal{T}} \bar{\kappa}$ and that the elemental edges are straight line segments.

The broken Laplacian, $\Delta_h u$, is defined by

$$(\Delta_h u)|_\kappa \quad = \quad \Delta(u|_\kappa) \qquad \forall \kappa \in \mathcal{T} \, .$$

Also, for a nonnegative integer r, we denote by $\mathcal{P}_r(\hat{\kappa})$, the set of all polynomials of total degree at most r, if $\hat{\kappa}$ is the reference triangle, or the set of all tensor-product polynomials on $\hat{\kappa}$ of degree at most r in each coordinate direction, if $\hat{\kappa}$ is the reference quadrilateral. For $r \geq 2$, we consider the finite element space

$$S_h^r := \{v \in L^2(\Omega) : v|_\kappa \circ F_\kappa \in \mathcal{P}_r(\hat{\kappa}),\, \kappa \in \mathcal{T}\}.$$

We shall assume throughout that the families of meshes considered are locally quasiuniform, i.e., there exists constant $c \geq 1$, independent of $\mathbf{h}$, such that, for any pair of elements κ^+ and κ^- in $\mathcal{T}$ which share an edge,

$$c^{-1} \leq h_{\kappa^+}/h_{\kappa^-} \leq c.$$

By Γ we denote the union of all one-dimensional element edges associated with the subdivision $\mathcal{T}$ (including the boundary). Further we decompose Γ into two disjoint subsets $\Gamma = \Gamma_\partial \cup \Gamma_{\text{int}}$, where $\Gamma_{\text{int}} := \Gamma \backslash \Gamma_\partial$.

Let κ^+, κ^- be two (generic) elements sharing an edge $e := \partial\kappa^+ \cap \partial\kappa^- \subset \Gamma_{\text{int}}$. Define the outward normal unit vectors $\mathbf{n}^+$ and $\mathbf{n}^-$ on e corresponding to $\partial\kappa^+$ and $\partial\kappa^-$, respectively. For functions $v : \Omega \to \mathbb{R}$ and $\mathbf{q} : \Omega \to \mathbb{R}^2$ that may be discontinuous across Γ, we define the following quantities. For $v^+ := v|_{e \subset \partial\kappa^+}$, $v^- := v|_{e \subset \partial\kappa^-}$, $\mathbf{q}^+ := \mathbf{q}|_{e \subset \partial\kappa^+}$, and $\mathbf{q}^- := \mathbf{q}|_{e \subset \partial\kappa^-}$, we set

$$\{v\} := \frac{1}{2}(v^+ + v^-), \; \{\mathbf{q}\} := \frac{1}{2}(\mathbf{q}^+ + \mathbf{q}^-),$$

and

$$[\![v]\!] := q^+\mathbf{n}^+ + q^-\mathbf{n}^-,\ [\mathbf{q}] := \mathbf{q}^+ \cdot \mathbf{n}^+ + \mathbf{q}^- \cdot \mathbf{n}^-;$$

if $e \in \partial\kappa \cap \Gamma_\partial$, these definitions are modified as follows

$$\{v\} := v^+,\ \{\mathbf{q}\} := \mathbf{q}^+,\ [\![v]\!] := v^+\mathbf{n},\ [\mathbf{q}] := \mathbf{q}^+ \cdot \mathbf{n}.$$

With the above definitions, it is easy to verify the identity

$$\sum_{\kappa\in\mathcal{T}} \int_{\partial\kappa} v\,\mathbf{q}\cdot\mathbf{n}_\kappa \,\mathrm{d}s = \int_\Gamma [\![v]\!]\cdot\{\mathbf{q}\}\,\mathrm{d}s + \int_{\Gamma_{\mathrm{int}}} \{v\}[\mathbf{q}]\,\mathrm{d}s. \tag{3}$$

2.3 The discontinuous Galerkin finite element method

In this section we present the IPDG finite element method for the model problem (1), (2). Firstly, we introduce the lifting operator $\mathcal{L} : \mathcal{S} := S_h^r + H_0^2(\Omega) \to S_h^r$ by

$$\int_\Omega \mathcal{L}(v) r \,\mathrm{d}x = \int_\Gamma \Big([\![v]\!]\cdot\{\nabla r\} - \{r\}[\nabla v] \Big)\,\mathrm{d}s \quad \forall r \in S_h^r. \tag{4}$$

Then, the *(symmetric) IPDG method* is defined by:

$$\text{find } u_h \in S_h^r \text{ such that} \quad B(u_h, v) = l(v_h) \quad \forall v_h \in S_h^r, \tag{5}$$

where the bilinear form $B : \mathcal{S}\times\mathcal{S} \to \mathbb{R}$ and the linear form $l : \mathcal{S} \to \mathbb{R}$ are given, respectively, by

$$\begin{aligned} B(w,v) = &\int_\Omega \Big(\Delta_h w \Delta_h v + \mathcal{L}(w)\Delta_h v + \Delta_h w \mathcal{L}(v) \Big)\,\mathrm{d}x \\ &+ \int_\Gamma \Big(\sigma [\![w]\!]\cdot[\![v]\!] + \tau [\nabla w][\nabla v] \Big)\,\mathrm{d}s, \end{aligned} \tag{6}$$

and

$$l(v) = \int_\Omega f v \,\mathrm{d}x, \tag{7}$$

for any $w, v \in \mathcal{S}$. Note that this formulation is inconsistent for trial and test functions belonging to the solution space $\mathcal{S}$. However, when $u_h, v_h \in S_h^r$, in view of (4), (6) gives

$$\begin{aligned} B(u_h, v_h) = &\int_\Omega \Delta_h u_h \Delta_h v_h \,\mathrm{d}x + \int_\Gamma \Big(\{\nabla\Delta u_h\}\cdot[\![v_h]\!] + \{\nabla\Delta v_h\}\cdot[\![u_h]\!] \\ &- \{\Delta u_h\}[\nabla v_h] - \{\Delta v_h\}[\nabla u_h] + \sigma [\![u_h]\!]\cdot[\![v_h]\!] + \tau [\nabla u_h][\nabla v_h] \Big)\,\mathrm{d}s; \end{aligned} \tag{8}$$

therefore, (5) coincides with the symmetric version of the interior penalty method presented in [25]. In practice, the right-hand side is approximated by L^2-projection of the source function f onto the finite element space S_h^r; we denote the L^2-projection of f onto S_h^r by Πf.

Here, the piecewise constant interior penalty parameters $\sigma, \tau : \Gamma \to \mathbb{R}$ are defined by

$$\sigma|_e = \sigma_0 (\mathbf{h}|_e)^{-3}, \quad \tau|_e = \tau_0 (\mathbf{h}|_e)^{-1}, \tag{9}$$

respectively, where $\sigma_0 > 0$ and $\tau_0 > 0$. To guarantee the stability of the IPDG method defined in (5), σ_0 and τ_0 must be selected sufficiently large, cf. [17] for details.

For any function $w \in \mathcal{S}$ the energy norm associated with $B(\cdot,\cdot)$ is defined by

$$|||w||| \quad = \quad (||\Delta_h w||_\Omega^2 + ||\sqrt{\sigma}[\![w]\!]||_\Gamma^2 + ||\sqrt{\tau}[\nabla w]||_\Gamma^2)^{\frac{1}{2}}. \tag{10}$$

Finally, we recall the following stability bound for the lifting operator $\mathcal{L}$: for $w \in \mathcal{S}$, we have

$$\|\mathcal{L}(w)\|_\Omega^2 \leq C\big(\|\sqrt{\sigma}[\![w]\!]\|_\Gamma^2 + \|\sqrt{\tau}[\nabla w]\|_\Gamma^2\big), \tag{11}$$

where C is a positive constant, independent of u_h and $\mathbf{h}$; the proof of this result can be found in [17].

3 Recovery operator

In the a posteriori analysis below, we shall make use of a recovery operator mapping elements of S_h^r onto a C^1-conforming space consisting of macro-elements of degree $r+2$. The family of macro-elements considered below will be high order versions of the classical Hsieh-Clough-Tocher macro-element, constructed in [13]. This mapping is constructed via averages of the nodal basis functions; cf. [21, 20, 7].

We recall the definition of the high-order C^1-conforming macro-elements constructed in [13].

Definition 3.1 *Let element $\kappa \in \mathcal{T}$. For $m \geq 4$, a macro-element of degree m is a nodal finite element $(\kappa, \tilde{\mathcal{P}}_m, \tilde{\mathcal{N}}_m)$, consisting of subtriangles κ_i, $i = 1, 2, \ldots, s$, with $s = 3$ if κ is a triangle, or $s = 4$ if κ is a quadrilateral (see Figures 1, 2, 3, 4 for an illustration). The local element space $\tilde{\mathcal{P}}_m$ is defined by*

$$\tilde{\mathcal{P}}_m := \{v \in C^1(\kappa) : v|_{\kappa_i} \in \mathcal{P}_m(\kappa_i),\ i = 1, \ldots, s\}.$$

The degrees of freedom $\tilde{\mathcal{N}}_m$ are defined as follows:

- *the value and the first (partial) derivatives at the vertices of κ;*
- *the value at $m-3$ distinct points in the interior of each exterior edge of κ;*
- *the normal derivative at $m-2$ distinct points in the interior of each exterior edge of κ;*
- *the value and the first (partial) derivatives at the common vertex of all κ_i, $i = 1, \ldots, s$;*
- *the value at $m-4$ distinct points in the interior of each edge of the κ_i, $i = 1, \ldots, s$ that is not an edge of κ;*
- *if κ is a triangle, the normal derivative at $m-4$ distinct points in the interior of each edge of the κ_i, $i = 1, \ldots, 3$ that is not an edge of κ; if κ is a quadrilateral, the normal derivative at $m-4$ distinct points in the interior of each edge of the κ_i, $i = 1, \ldots, 4$ that is not an edge of κ* and *an extra normal derivative at a point in the interior of just one of the edges of the κ_i that is not an edge of κ.*

The corresponding finite element space consisting of the above macro-elements will be denoted by $\tilde{S}_h^m$.

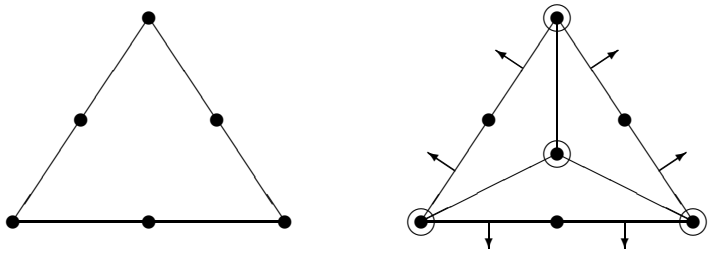

Figure 1: $\mathcal{P}_2$ Lagrange triangular element and $\tilde{\mathcal{P}}_4$ C^1-conforming macro-element

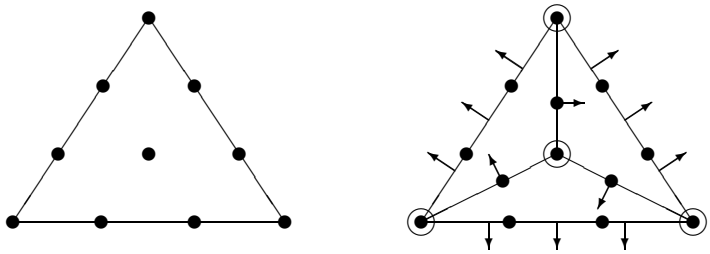

Figure 2: $\mathcal{P}_3$ Lagrange triangular element and $\tilde{\mathcal{P}}_5$ C^1-conforming macro-element

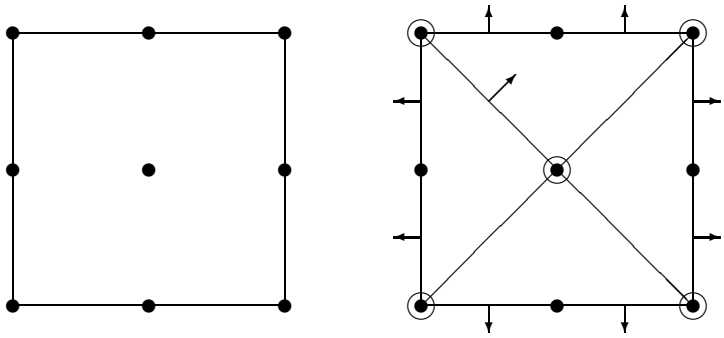

Figure 3: $\mathcal{P}_2$ Lagrange quadrilateral element and $\tilde{\mathcal{P}}_4$ C^1-conforming macro-element

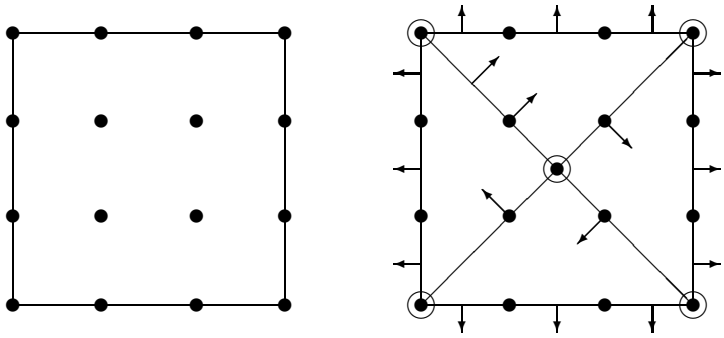

Figure 4: $\mathcal{P}_3$ Lagrange quadrilateral element and $\tilde{\mathcal{P}}_5$ C^1-conforming macro-element

The case $m = 3$, corresponding to the classical Hsieh-Clough-Tocher element (see, e.g., [10]), is not considered here as it is not relevant to the subsequent discussion.

Let us consider the standard Lagrange basis for a polynomial of degree r, $r \geq 2$ (depicted for $r = 2, 3$ for triangles and quadrilaterals on the left-hand side in Figures 1, 2, 3, 4, respectively). A crucial observation here is that *the set of the nodal points of the Lagrange basis is a subset of the set of the nodal points of the macro-element of degree* $r + 2$.

Lemma 3.1 *Assume that the mesh* $\mathcal{T}$ *is constructed as in Section 2.2. Then, there exists an operator* $E : S_h^r \to \tilde{S}_h^{r+2} \cap H_0^2(\Omega)$*, satisfying the following bound*

$$\sum_{\kappa \in \mathcal{T}} |u_h - E(u_h)|^2_{\alpha,\kappa} \leq C \left(||\mathbf{h}^{1/2-\alpha} [\![u_h]\!]||^2_\Gamma + ||\mathbf{h}^{3/2-\alpha} [\nabla u_h]||^2_\Gamma \right), \tag{12}$$

with $\alpha = 0, 1, 2$ *and* $C > 0$ *a constant independent of* $\mathbf{h}$ *and* u_h*. (The notational convention* $\|w\|_\kappa \equiv |w|_{0,\kappa}$ *for* $w \in L^2(\kappa)$ *is adopted here and in the sequel.)*

Proof For each nodal point ν of the C^1-conforming finite element space $\tilde{S}_h^{r+2}$, we define ω_ν to be the set of $\kappa \in \mathcal{T}$ which share the nodal point ν, i.e.,

$$\omega_\nu := \{\kappa \in \mathcal{T} : \nu \in \kappa\};$$

also, $|\omega_\nu|$ will denote the cardinality of ω_ν. We notice that if ν is located in the interior of an element, we have $|\omega_\nu| = 1$. We define the operator $E : S_h^r \to \tilde{S}_h^{r+2} \cap H_0^2(\Omega)$, by

$$N_\nu(E(u_h)) = \begin{cases} \dfrac{1}{|\omega_\nu|} \displaystyle\sum_{\kappa \in \omega_\nu} N_\nu(u_h|_\kappa) & , \quad \text{if } \nu \notin \Gamma_\partial; \\ 0 & , \quad \text{if } \nu \in \Gamma_\partial. \end{cases}$$

here N_ν is any nodal variable at ν and ν is any nodal point of $\tilde{S}_h^{r+2}$. Note that $N_\nu(E(u_h)) = N_\nu(u_h)$ if ν is in the interior of an element. We denote by $\mathcal{N}$ the set of all nodal variables of $\tilde{S}_h^{r+2}$ *defined on every element of* $\mathcal{T}$ (i.e., they may be discontinuous across element boundaries) and we split $\mathcal{N}$ into two subsets $\mathcal{N}_0$ and $\mathcal{N}_1$ consisting of the nodal variables corresponding to function evaluations, and those involving partial and normal derivatives of the function, respectively.

An inverse estimate gives,

$$\sum_{\kappa \in \mathcal{T}} |u_h - E(u_h)|^2_{\alpha,\kappa} \leq C ||\mathbf{h}^{-\alpha}(u_h - E(u_h))||^2_\Omega,$$

or a positive constant C, which is independent of $\mathbf{h}$ and u_h. The equivalence of norms in a finite dimensional vector space, along with a scaling argument yields

$$||\mathbf{h}^{-\alpha}(u_h - E(u_h))||^2_\Omega \leq C \sum_{i=0}^{1} \sum_{\substack{N_\nu \in \mathcal{N}_i \\ \nu \in \kappa}} h_\kappa^{2(i+1-\alpha)} \big(N_\nu(u_h - E(u_h))\big)^2.$$

For each nodal point ν that is not on the boundary Γ_∂, we consider a local numbering $\kappa_1, \ldots, \kappa_{|\omega_\nu|-1}$ of the elements in ω_ν, so that each consecutive pair κ_j, κ_{j+1} shares an edge.

Recalling the arithmetic-geometric mean inequality (cf. Lemma 2.2 [21]), we have that

$$\begin{aligned}
&\sum_{\substack{N_\nu \in \mathcal{N}_0 \\ \nu \in \kappa}} h_\kappa^{2(1-\alpha)} \big(N_\nu(u_h - E(u_h))\big)^2 \\
&= \sum_{\substack{N_\nu \in \mathcal{N}_0 \\ \nu \in \kappa \cap \Gamma_{\text{int}}}} h_\kappa^{2(1-\alpha)} \Big(u_h(\nu)|_\kappa - \frac{1}{|\omega_\nu|} \sum_{\kappa \in \omega_\nu} u_h(\nu)|_\kappa\Big)^2 + \sum_{\substack{N_\nu \in \mathcal{N}_0 \\ \nu \in \kappa \cap \Gamma_\partial}} h_\kappa^{2(1-\alpha)} \Big(u_h(\nu)|_\kappa\Big)^2 \\
&\leq C \sum_{\substack{N_\nu \in \mathcal{N}_0 \\ \nu \in \kappa \cap \Gamma_{\text{int}}}} h_\kappa^{2(1-\alpha)} \Big(\sum_{j=1}^{|\omega_\nu|-1} \big(u_h|_{\kappa_j}(\nu) - u_h|_{\kappa_{j+1}}(\nu)\big)^2 \Big) + \sum_{\substack{N_\nu \in \mathcal{N}_0 \\ \nu \in \kappa \cap \Gamma_\partial}} h_\kappa^{2(1-\alpha)} \Big(u_h(\nu)|_\kappa\Big)^2 \\
&\leq C \sum_{e \in \Gamma} ||\mathbf{h}^{1-\alpha} [\![u_h]\!]||^2_{L^\infty(e)} \leq C \sum_{e \in \Gamma} ||\mathbf{h}^{1/2-\alpha} [\![u_h]\!]||^2_e.
\end{aligned} \tag{13}$$

We now turn to the nodal variables in $\mathcal{N}_1$, which we further split into $\mathcal{N}_1^n$ and $\mathcal{N}_1^p$, the set of the nodal variables of normal derivatives across element edges and the set of nodal variables representing partial derivatives on elemental vertices, respectively.

For $\mathcal{N}_1^n$, the argument is analogous to (13):

$$\begin{aligned}
&\sum_{\substack{N_\nu \in \mathcal{N}_1^n \\ \nu \in \kappa}} h_\kappa^{2(2-\alpha)} \big(N_\nu(u_h - E(u_h))\big)^2 \\
&\qquad \leq C \sum_{\substack{N_\nu \in \mathcal{N}_1^n \\ \nu \in \kappa_1 \cap \kappa_2}} h_{\kappa_1}^{2(2-\alpha)} \big((\nabla u_h \cdot \mathbf{n}_{\kappa_1})|_{\kappa_1}(\nu) - (\nabla u_h \cdot \mathbf{n}_{\kappa_2})|_{\kappa_2}(\nu)\big)^2 \\
&\qquad\quad + \sum_{\substack{N_\nu \in \mathcal{N}_1^n \\ \nu \in \kappa \cap \Gamma_\partial}} h_\kappa^{2(2-\alpha)} \Big((\nabla u_h \cdot \mathbf{n})|_\kappa(\nu)\Big)^2 \\
&\qquad \leq C \sum_{e \in \Gamma} ||\mathbf{h}^{2-\alpha} [\nabla u_h]||^2_{L^\infty(e)} \leq C \sum_{e \in \Gamma} ||\mathbf{h}^{3/2-\alpha} [\nabla u_h]||^2_e.
\end{aligned}$$

For $\mathcal{N}_1^p$, the first part of the argument is also analogous to (13), yielding

$$\sum_{\substack{N_\nu \in \mathcal{N}_1^p \\ \nu \in \kappa}} h_\kappa^{2(2-\alpha)} \big(N_\nu(u_h - E(u_h))\big)^2 \leq C \sum_{e \in \Gamma} \sum_{z \in \{x,y\}} ||\mathbf{h}^{3/2-\alpha} [\![(u_h)_z]\!]||^2_e. \tag{14}$$

Splitting the partial derivatives on the right-hand side of (14) into normal and tangential components, and using an inverse estimate along each edge e for the tangential derivative component, in conjunction with the fact that the edges e are straight lines, gives

$$\begin{aligned}
||\mathbf{h}^{3/2-\alpha} [\![(u_h)_z]\!]||^2_e \leq& 2||\mathbf{h}^{3/2-\alpha} [\nabla u_h]||^2_e + 2||\mathbf{h}^{3/2-\alpha} [\![(u_h)_t]\!]||^2_e \\
\leq& 2||\mathbf{h}^{3/2-\alpha} [\nabla u_h]||^2_e + C||\mathbf{h}^{1/2-\alpha} [\![u_h]\!]||^2_e,
\end{aligned}$$

where $(\cdot)_t$ denotes the tangential derivative along the edge e.

The proof is completed by combining the above bounds.

□

4 A posteriori error bounds

In the following theorem we establish a reliable a posteriori error bound in the case when the analytical solution u of (1), (2) satisfies $u \in H_0^2(\Omega)$.

Theorem 4.1 *Let $u \in H_0^2(\Omega)$ be the solution to (1), (2), $u_h \in S_h^r$ be the approximation obtained by the DG method and σ and τ as in (9). Then there exists a positive constant C, independent of $\mathbf{h}$, u and u_h, so that*

$$\begin{aligned}|||u-u_h|||^2 \leq & C\Big(||\mathbf{h}^2(\Pi f-\Delta_h^2 u_h)||_\Omega^2+||\mathbf{h}^2(f-\Pi f)||_\Omega^2+C_p\Big(||\mathbf{h}^{-3/2}[\![u_h]\!]||_\Gamma^2 \\ & +||\mathbf{h}^{-1/2}[\nabla u_h]||_\Gamma^2\Big)+||\mathbf{h}^{1/2}[\![\Delta u_h]\!]||_{\Gamma_{\text{int}}}^2+||\mathbf{h}^{3/2}[\nabla\Delta u_h]||_{\Gamma_{\text{int}}}^2\Big),\end{aligned} \tag{15}$$

with $C_p := \max\{1,\sigma_0,\tau_0,\sigma_0^2,\tau_0^2\}$.

Proof Let $v_h \in S_h^r$, $v \in H_0^2(\Omega)$, $\eta = v - v_h$ and $E(u_h) \in \tilde{S}_h^{r+2} \cap H_0^2(\Omega)$ be as in Lemma 3.1. With this notation, we decompose the error as follows

$$e := u - u_h = (u - E(u_h)) + (E(u_h) - u_h) \equiv e^c + e^d\,.$$

Since u is the solution to the weak problem, we have $B(u,v) = l(v)$, as $\mathcal{L}(u) = \mathcal{L}(v) = 0$. Hence,

$$B(e,v) = B(u,v) - B(u_h,v) = l(v) - B(u_h, v-v_h) - B(u_h,v_h) = l(\eta) - B(u_h,\eta) \tag{16}$$

and, thus

$$B(e^c,v) = l(\eta) - B(u_h,\eta) - B(e^d,v)\,. \tag{17}$$

Next, we note that $\mathcal{L}(e^c) = 0$ as $e^c \in H_0^2(\Omega)$ and therefore, upon setting $v = e^c$ in (17), we deduce that

$$||\Delta e^c||^2 = B(e^c,e^c) = l(\eta) - B(u_h,\eta) - B(e^d,e^c)\,. \tag{18}$$

Since $\mathcal{L}(e^c) = [\![e^c]\!] = [\nabla e^c] = 0$, we obtain

$$\begin{aligned}|B(e^d,e^c)| = & \Big|\int_\Omega \big(\Delta_h e^d \Delta e^c + \mathcal{L}(e^d)\Delta e^c\big)\,\mathrm{d}x\Big| \\ \leq & \Big(||\Delta_h e^d||_\Omega^2 + C\big(||\sqrt{\sigma}[\![u_h]\!]||_\Gamma^2 + ||\sqrt{\tau}[\nabla u_h]||_\Gamma^2\big)\Big)^{1/2} ||\Delta e^c||_\Omega\end{aligned} \tag{19}$$

using the stability of the lifting operator (11).

After integration by parts, the first two terms on the right-hand side in (18) become

$$\begin{aligned}l(\eta) - B(u_h,\eta) = & \int_\Omega (f-\Delta_h^2 u_h)\eta\,\mathrm{d}x - \int_\Omega \big(\mathcal{L}(\eta)\Delta_h u_h + \mathcal{L}(u_h)\Delta_h\eta\big)\,\mathrm{d}x \\ & - \sum_{\kappa\in\mathcal{T}}\int_{\partial\kappa}\big(\Delta_h u_h \mathbf{n}_\kappa\cdot\nabla\eta - \nabla\Delta u_h\cdot\mathbf{n}_\kappa\eta\big)\,\mathrm{d}s \\ & - \int_\Gamma \big(\sigma[\![u_h]\!]\cdot[\![\eta]\!] + \tau[\nabla u_h][\nabla\eta]\big)\,\mathrm{d}s\,.\end{aligned} \tag{20}$$

As $u_h, v_h \in S_h^r$ and $v \in H_0^2(\Omega)$, we can use the definition of the lifting operator, to obtain

$$\int_\Omega \mathcal{L}(\eta)\Delta_h u_h\,\mathrm{d}x = \int_\Gamma \big([\![\eta]\!]\cdot\{\nabla\Delta u_h\} - \{\Delta_h u_h\}[\nabla\eta]\big)\,\mathrm{d}s. \tag{21}$$

Employing the identity (3) on the third term on the right-hand side of (20) gives

$$\begin{aligned}\sum_{\kappa\in\mathcal{T}}\int_{\partial\kappa}\left(\Delta_h u_h\mathbf{n}_\kappa\cdot\nabla\eta-\nabla\Delta u_h\cdot\mathbf{n}_\kappa\eta\right)\mathrm{d}s=&\int_\Gamma[\nabla\eta]\{\Delta_h u_h\}\,\mathrm{d}s+\int_{\Gamma_{\text{int}}}\{\nabla\eta\}\cdot[\![\Delta_h u_h]\!]\,\mathrm{d}s\\&-\int_\Gamma[\![\eta]\!]\cdot\{\nabla\Delta u_h\}\,\mathrm{d}s-\int_{\Gamma_{\text{int}}}\{\eta\}[\nabla\Delta u_h]\,\mathrm{d}s\,.\end{aligned}\tag{22}$$

Inserting (21) and (22) into (20), we deduce that

$$\begin{aligned}l(\eta)-B(u_h,\eta)=&\int_\Omega\left((f-\Delta^2u_h)\eta-\mathcal{L}(u_h)\Delta_h\eta\right)\mathrm{d}x+\int_{\Gamma_{\text{int}}}\{\eta\}[\nabla\Delta_h u_h]\,\mathrm{d}s\\&-\int_{\Gamma_{\text{int}}}\{\nabla\eta\}\cdot[\![\Delta_h u_h]\!]\,\mathrm{d}s-\int_\Gamma\left(\sigma[\![u_h]\!]\cdot[\![\eta]\!]+\tau[\nabla u_h][\nabla\eta]\right)\mathrm{d}s\,.\end{aligned}\tag{23}$$

Fix v_h to be the elementwise linear approximation to e^c such that

$$|e^c-v_h|_{j,\kappa}\leq Ch_\kappa^{m-j}|e^c|_{m,\kappa}\tag{24}$$

for $C>0$, independent of $\mathcal{T}$, for $0\leq j\leq m\leq 2$, $\kappa\in\mathcal{T}$. We shall use this to bound the terms on the right-hand side of (23) and (19).

For the first term on the right-hand side of (23), we use (24) and the stability of the lifting operator (11), to deduce

$$\begin{aligned}\Big|\int_\Omega\left((f-\Delta_h^2u_h)\eta-\mathcal{L}(u_h)\Delta_h\eta\right)\mathrm{d}x\Big|\leq&C\Big(||\mathbf{h}^2(f-\Delta_h^2u_h)||_\Omega^2\\&+||\sqrt{\sigma}[\![u_h]\!]||_\Gamma^2+||\sqrt{\tau}[\nabla u_h]||_\Gamma^2\Big)^{1/2}|e^c|_{2,\Omega}.\end{aligned}\tag{25}$$

Using the bound

$$||\mathbf{h}^{-3/2}\{\eta\}||_{\Gamma_{\text{int}}}^2\leq C\sum_{\kappa\in\mathcal{T}}h_\kappa^{-3}||\eta||_{\partial\kappa}^2\leq C\sum_{\kappa\in\mathcal{T}}h_\kappa^{-3}(h_\kappa^{-1}||\eta||_\kappa^2+h_\kappa|\eta|_{1,\kappa}^2)\leq C|e^c|_{2,\Omega}^2,$$

the second term on the right-hand side of (23) can be bounded as follows

$$\Big|\int_{\Gamma_{\text{int}}}\{\eta\}[\nabla\Delta_h u_h]\,\mathrm{d}s\Big|\leq C||\mathbf{h}^{3/2}[\nabla\Delta u_h]||_{\Gamma_{\text{int}}}|e^c|_{2,\Omega}.\tag{26}$$

Similarly, using the bound

$$||\mathbf{h}^{-1/2}\{\nabla\eta\}||_{\Gamma_{\text{int}}}^2\leq C\sum_{\kappa\in\mathcal{T}}h_\kappa^{-1}||\nabla\eta||_{\partial\kappa}^2\leq C\sum_{\kappa\in\mathcal{T}}h_\kappa^{-1}(h_\kappa^{-1}|\eta|_{1,\kappa}^2+h_\kappa|\eta|_{2,\kappa}^2),\leq C|e^c|_{2,\Omega}^2,$$

the third term on the right-hand side of (23) can be bounded as follows

$$\Big|\int_{\Gamma_{\text{int}}}\{\nabla\eta\}\cdot[\![\Delta_h u_h]\!]\,\mathrm{d}s\Big|\leq||\mathbf{h}^{1/2}[\![\Delta u_h]\!]||_{\Gamma_{\text{int}}}|e^c|_{2,\Omega}.\tag{27}$$

For the penalty terms we work in a similar fashion, to deduce

$$\Big|\int_\Gamma\left(\sigma[\![u_h]\!]\cdot[\![\eta]\!]+\tau[\nabla u_h][\nabla\eta]\right)\mathrm{d}s\Big|\leq CC_p\big(||\mathbf{h}^{-3/2}[\![u_h]\!]||_\Gamma^2+||\mathbf{h}^{-1/2}[\nabla u_h]||_\Gamma^2\big)^{1/2}|e^c|_{2,\Omega}.\tag{28}$$

Observing that $|e^c|_{2,\Omega} = ||\Delta e^c||_\Omega$, since $e^c \in H_0^2(\Omega)$, and using the bounds (19), (25), (26), (27) and (28) on (18) gives

$$\begin{aligned} ||\Delta e^c||_\Omega^2 \leq & C\Big(||\mathbf{h}^2(f - \Delta_h^2 u_h)||_\Omega^2 + C_p\Big(||\mathbf{h}^{-3/2}[\![u_h]\!]||_\Gamma^2 + ||\mathbf{h}^{-1/2}[\nabla u_h]||_\Gamma^2 \Big) \\ & + ||\mathbf{h}^{1/2}[\![\Delta u_h]\!]||_\Gamma^2 + ||\mathbf{h}^{3/2}[\nabla \Delta u_h]||_\Gamma^2 + ||\Delta_h e^d||_\Omega^2 \Big). \end{aligned} \tag{29}$$

Finally, employing the triangle inequality

$$||\Delta_h e||_\Omega \leq ||\Delta e^c||_\Omega + ||\Delta_h e^d||_\Omega,$$

in conjunction with Lemma 3.1 completes the proof.

□

Next we prove the efficiency of the estimator.

Theorem 4.2 *Under the foregoing assumptions stated in Theorem 4.1, there are positive constants c_1, c_2 and c_3, independent of $\mathbf{h}$ and u_h, such that for each element $\kappa \in \mathcal{T}$, we have*

$$||\mathbf{h}^2(\Pi f - \Delta^2 u_h)||_\kappa^2 \leq c_1\big(||\Delta e||_\kappa^2 + ||\mathbf{h}^2(f - \Pi f)||_\kappa^2\big), \tag{30}$$

and for each edge $e \in \Gamma_{\text{int}}$ we have

$$||\mathbf{h}^{1/2}[\![\Delta u_h]\!]||_e^2 \leq c_2\big(||\Delta_h e||_{\kappa_1 \cup \kappa_2}^2 + ||\mathbf{h}^2(f - \Pi f)||_{\kappa_1 \cup \kappa_2}^2\big), \tag{31}$$

and

$$||\mathbf{h}^{3/2}[\nabla \Delta u_h]||_e^2 \leq c_3\big(||\Delta_h e||_{\kappa_1 \cup \kappa_2}^2 + ||\mathbf{h}^2(f - \Pi f)||_{\kappa_1 \cup \kappa_2}^2\big), \ . \tag{32}$$

where κ_1 and κ_2 denote two elements such that $e = \kappa_1 \cap \kappa_2$.

Proof Fix $\kappa \in \mathcal{T}$ and let $v \in H_0^2(\Omega) \cap H_0^2(\kappa)$, with $v = 0$ on $\Omega \backslash \kappa$, be a polynomial function on κ (to be defined later). Setting $v_h = 0$ and taking v as above in (16) yields

$$\int_\kappa \Delta e \Delta v \, \mathrm{d}x = \int_\kappa \big(f - \Delta^2 u_h\big) v \, \mathrm{d}x = \int_\kappa (\Pi f - \Delta^2 u_h) v \, \mathrm{d}x + \int_\kappa (f - \Pi f) v \, \mathrm{d}x, \tag{33}$$

noting that $[\![v]\!] = [\nabla v] = \{v\} = \{\nabla v\} = 0$ on Γ and that $\mathcal{L}(u) = \mathcal{L}(v) = 0$ on Ω. Hence, we have that

$$\begin{aligned} \int_\kappa (\Pi f - \Delta^2 u_h) v \, \mathrm{d}x \leq & ||\Delta e||_\kappa ||\Delta v||_\kappa + ||\Pi f - f||_\kappa ||v||_\kappa \\ \leq & C\big(||\Delta e||_\kappa + ||\mathbf{h}^2(\Pi f - f)||_\kappa\big) ||\mathbf{h}^{-2} v||_\kappa. \end{aligned} \tag{34}$$

We set $v|_\kappa = (\Pi f - \Delta^2 u_h) b_\kappa^2$, where $b_\kappa : \kappa \to \mathbb{R}$ is the standard interior "bubble" function (which is defined by $b_\kappa := b_{\hat{\kappa}} \circ F_\kappa$, where $b_{\hat{\kappa}} := 27\lambda_1\lambda_2\lambda_3$, if $\hat{\kappa}$ is the reference triangle with barycentric coordinates $\lambda_1, \lambda_2, \lambda_3$, and $b_{\hat{\kappa}} := (1-\lambda_1^2)(1-\lambda_2^2)$ if $\hat{\kappa}$ is the reference rectangle with λ_1 and λ_2 its corresponding coordinates). We note that $||(\cdot) b_\kappa||_\kappa$ defines a norm on the finite dimensional space $\mathcal{P}_{r+2}(\kappa)$. This norm is, therefore, equivalent to $||\cdot||_\kappa$ on $\mathcal{P}_{r+2}(\kappa)$. A scaling argument reveals that the equivalence constants are independent of $\mathbf{h}$; in particular, we have

$$||\Pi f - \Delta^2 u_h||_\kappa^2 \leq C \int_\kappa (\Pi f - \Delta^2 u_h)^2 b_\kappa^2 \, \mathrm{d}x = C \int_\kappa (\Pi f - \Delta^2 u_h) v \, \mathrm{d}x. \tag{35}$$

Combining (34) with (35) gives (30).

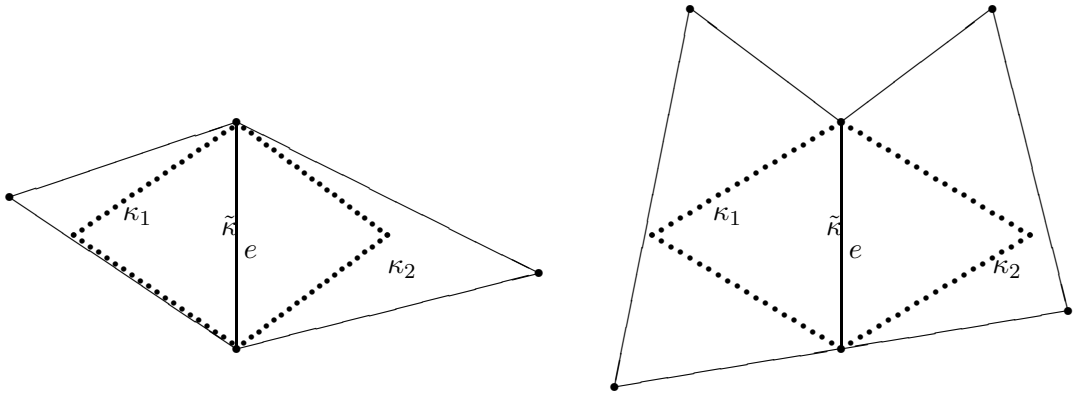

(a) (b)

Figure 5: Inscribed rhombus $\tilde{\kappa}$ for: (a) Triangular elements; (b) Quadrilateral elements.

Next, for each internal edge $e \in \Gamma_{\text{int}}$, we define $\tilde{\kappa} \subset \kappa_1 \cup \kappa_2$, to be the largest rhombus contained in $\kappa_1 \cup \kappa_2$ that has e as one diagonal (see Figure 5). Also, we define $b_{\tilde{\kappa}} : \tilde{\kappa} \to \mathbb{R}$ to be the "bubble" function on the rhombus $\tilde{\kappa}$. Let also $b_l : \tilde{\kappa} \to \mathbb{R}$ to be an affine function (i.e., a piece of a plane) having value zero along the edge e, such that $\big(\nabla b_l \cdot \mathbf{n}\big)|_e = \mathbf{h}^{-2}|_e$, thereby defining b_l completely up to a sign, which is not relevant to the discussion. Using the above definitions, we consider the function $b_e : \Omega \to \mathbb{R}$, with $b_e|_{\tilde{\kappa}} := b_l b_{\tilde{\kappa}}^3$, and $b_e := 0$ on $\Omega \backslash \tilde{\kappa}$, which has the following properties:

$$\begin{aligned} &b_e \in C^2(\Omega) \cap H_0^2(\Omega), \quad [\![b_e]\!] = [\nabla b_e] = \{b_e\} = 0 \text{ on } \Gamma, \\ &\big(\{\nabla b_e\} \cdot \mathbf{n}\big)|_e = \big(\mathbf{h}^{-2} b_{\tilde{\kappa}}^3\big)|_e \ \text{ and } \ \{\nabla b_e\} = 0 \text{ on } \Gamma \backslash e, \end{aligned} \tag{36}$$

observing that $\nabla b_{\tilde{\kappa}} \cdot \mathbf{n} = 0$ along the edge e.

We define $v = \phi b_e$ where ϕ is a constant function in the normal direction to e (i.e., $\big(\nabla \phi \cdot \mathbf{n}\big)|_e = 0$). For this v and for $v_h = 0$, (16) yields

$$\int_{\kappa_1 \cup \kappa_2} (f - \Delta_h^2 u_h) v \, \mathrm{d}x - \int_{\kappa_1 \cup \kappa_2} \Delta_h e \Delta_h v \, \mathrm{d}x = \int_e [\![\Delta u_h]\!] \cdot \{\nabla v\} \, \mathrm{d}s \, . \tag{37}$$

Setting $\phi|_e = \big([\![\Delta u_h]\!] \cdot \mathbf{n}\big)|_e$ in (37), we have

$$\int_e [\![\Delta u_h]\!] \cdot \{\nabla v\} \, \mathrm{d}s = ||b_{\tilde{\kappa}}^{3/2} \mathbf{h}^{-1} [\![\Delta u_h]\!]||_e^2 \geq C ||\mathbf{h}^{-1} [\![\Delta u_h]\!]||_e^2, \tag{38}$$

from a norm-equivalence and scaling argument.

Let then $l : e \to \mathbb{R}$, where $l(s)$ denotes the length of the intersection of the line normal to e, crossing e at the point $s \in e$, and $\tilde{\kappa}$. Then, we have

$$||v||_{\kappa_1 \cup \kappa_2} \leq C ||\phi||_{\kappa_1 \cup \kappa_2} = C \Big(\int_e \phi^2(s) l(s) \, \mathrm{d}s \Big)^{1/2} \leq C ||\mathbf{h}^{1/2} \phi||_e = C ||\mathbf{h}^{1/2} [\![\Delta u_h]\!]||_e. \tag{39}$$

From (37) and (38), we arrive to

$$||\mathbf{h}^{-1} [\![\Delta u_h]\!]||_e^2 \leq \big(||\mathbf{h}^2 (f - \Delta_h^2 u_h)||_{\kappa_1 \cup \kappa_2} + ||\Delta_h e||_{\kappa_1 \cup \kappa_2} \big) ||\mathbf{h}^{-2} v||_{\kappa_1 \cup \kappa_2}. \tag{40}$$

Using (39) and (30) in (40), the bound stated in (31) follows.

To estimate $[\nabla \Delta u_h]$, we first note that we have

$$b_{\tilde{\kappa}}^3 \in C^2(\Omega) \cap H_0^2(\Omega), \quad [\![b_{\tilde{\kappa}}^3]\!] = [\nabla b_{\tilde{\kappa}}^3] = \{\nabla b_{\tilde{\kappa}}^3\} \cdot \mathbf{n} = 0 \text{ on } \Gamma \ \text{ and } \ \{b_{\tilde{\kappa}}^3\} = 0 \text{ on } \Gamma \backslash e \, . \tag{41}$$

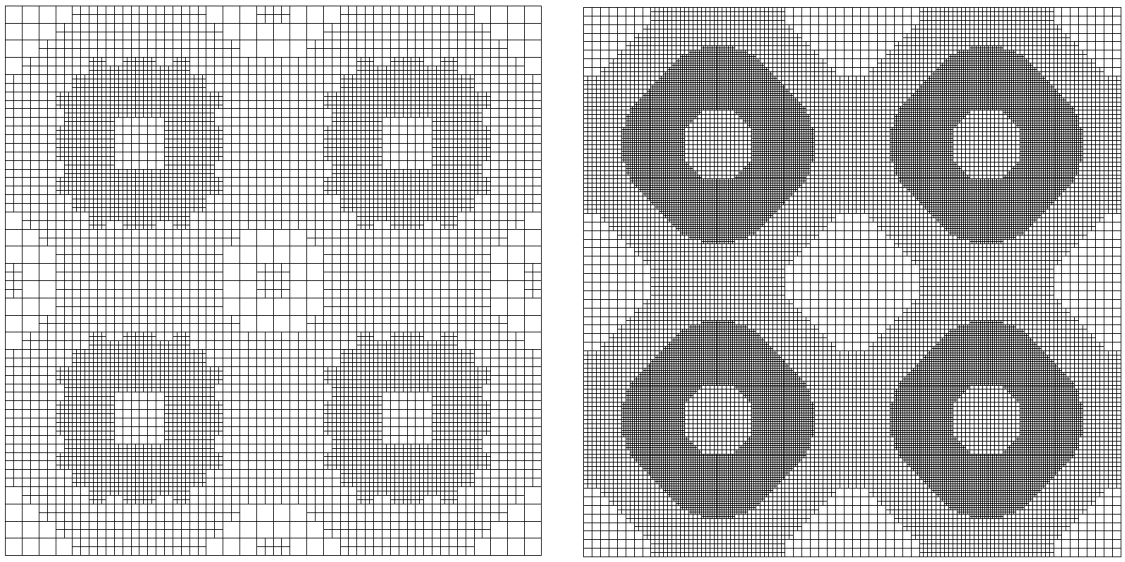

(a) (b)

Figure 6: *Example 1.* Computational mesh with: (a) 7300 elements, after 7 adaptive refinements; (b) 30208 elements, after 10 adaptive refinements;

We set $v = \psi b_{\bar{\kappa}}^3$, where ψ is a constant function in the normal direction to e. For this v and for $v_h = 0$, (16) yields

$$\int_{\kappa_1 \cup \kappa_2} (f - \Delta_h^2 u_h) v \, \mathrm{d}x - \int_{\kappa_1 \cup \kappa_2} \Delta_h e \Delta_h v \, \mathrm{d}x = \int_e [\nabla \Delta u_h] \{v\} \, \mathrm{d}s \, . \tag{42}$$

Setting $\psi|_e = [\nabla \Delta u_h]|_e$ in (42), and working similarly as above, the result follows.

□

5 Numerical Experiments

In this section we present a series of two-dimensional numerical examples to illustrate the practical performance of the proposed a posteriori error estimator within an automatic adaptive refinement procedure. In each of the examples shown below, we set the polynomial degree r equal to 2. The DG solution of (5) is computed using the interior penalty parameters $\sigma_0 = \tau_0 = 10$. The adaptive meshes are constructed by employing the fixed fraction strategy, with refinement and derefinement fractions set to 20% and 10%, respectively. Here, the emphasis will be to demonstrate that the proposed a posteriori error indicator converges to zero at the same asymptotic rate as the energy norm of the actual error on a sequence of non-uniform adaptively refined meshes. With this mind, as in [4], we set the constant C arising in Theorem 4.1 equal to one and ensure that the corresponding effectivity indices are roughly constant on all of the meshes employed; here, the effectivity index is defined as the ratio of the a posteriori error bound and the energy norm of the actual error. In general, to ensure the reliability of the error estimator, C must be determined numerically for the underlying problem at hand, cf. [15], for example.

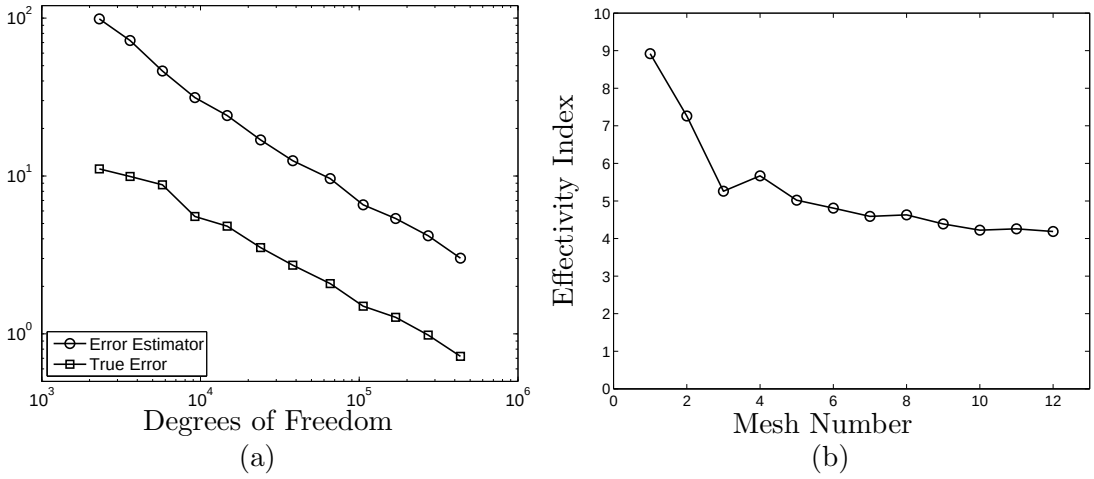

Figure 7: *Example 1.* (a) Comparison of the actual and estimated energy norm of the error with respect to the number of degrees of freedom; (b) Effectivity Indices.

5.1 Example 1

Here, we let $\Omega = (0,1)^2$ and select f so that the analytical solution to (1) and (2) is given by

$$u(x,y) = \sin(2\pi x)^2 \, \sin(2\pi y)^2;$$

this is a variant of the model problem considered in [25], cf. also [17].

In Figure 6 we show the mesh generated using the proposed a posteriori error indicator after 7 and 10 adaptive refinement steps. Here, we see that while the mesh has been largely uniformly refined throughout the entire computational domain, additional refinement has been performed where the gradient/curvature of the analytical solution is relativity large.

Finally, in Figure 7 we present a comparison of the actual and estimated energy norm of the error versus the number of degrees of freedom in the finite element space S_h^r, on the sequence of meshes generated by our adaptive algorithm. Here, we observe that there is an initial transient, whereby the effectivity index is relatively large. However, as the refinement algorithm proceeds, the error bound (asymptotically) over-estimates the true error by a consistent factor; indeed, from Figure 7(b), we see that the computed effectivity indices tend to a value of just over 4.

5.2 Example 2

In this second example, we investigate the performance of the interior penalty DG method (5) for a problem with a corner singularity in u. To this end, we let Ω be the L-shaped domain $(-1,1)^2 \setminus [0,1) \times (-1,0]$, and select $f = 0$. Then, writing (r,φ) to denote the system of polar coordinates, we impose an appropriate inhomogeneous boundary condition for u so that

$$u = r^{5/3} \sin(5\varphi/3).$$

The analytical solution u contains a singularity at the corner located at the origin of Ω; here, we only have $u \in H^{8/3-\varepsilon}(\Omega)$, $\varepsilon > 0$.

In Figure 8 we show the mesh generated using the local error indicators after 7 and 9 adaptive refinement steps. Here, we see that the mesh has been largely refined in the vicinity

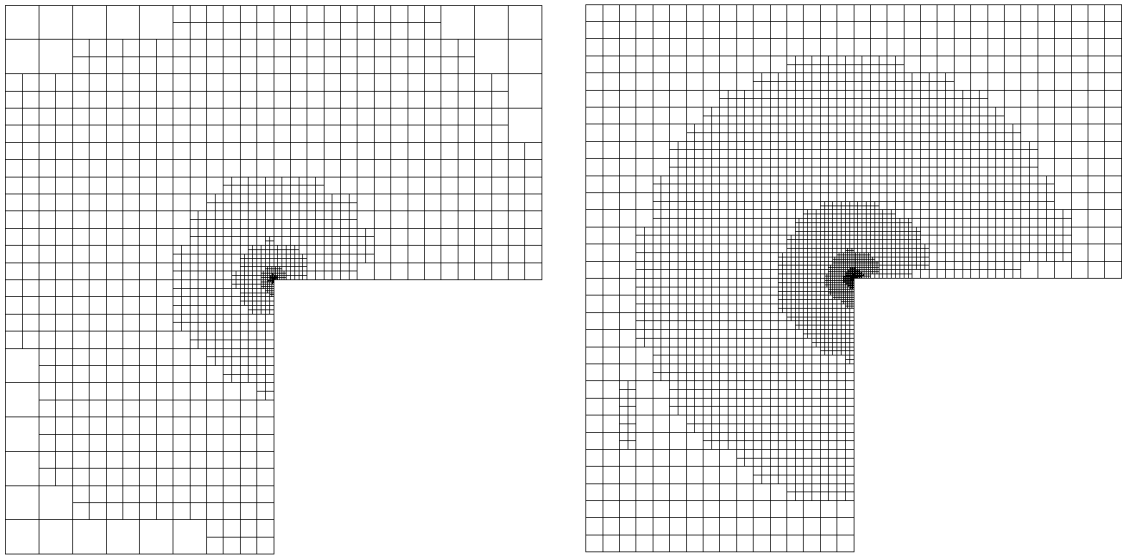

(a) (b)

Figure 8: *Example 2.* Computational mesh with: (a) 1248 elements, after 7 adaptive refinements; (b) 3198 elements, after 9 adaptive refinements;

of the re-entrant corner located at the origin, as well as in the region adjacent to this singular point. Finally, Figure 9 shows the history of the actual and estimated energy norm of the error on each of the meshes generated by our adaptive algorithm, together with their corresponding effectivity indices. As in the previous example, we observe that the a posteriori bound overestimates the true error by a consistent factor around 4.

References

[1] Ainsworth, M. A posteriori error estimation for discontinuous Galerkin finite element approximation. *SIAM J. Numer. Anal. 45*, 4 (2007), 1777–1798.

[2] Arnold, D. N., Brezzi, F., Cockburn, B., and Marini, L. D. Unified analysis of discontinuous Galerkin methods for elliptic problems. *SIAM J. Numer. Anal. 39*, 5 (2001/02), 1749–1779 (electronic).

[3] Baker, G. A. Finite element methods for elliptic equations using nonconforming elements. *Math. Comp. 31*, 137 (1977), 45–59.

[4] Becker, R., Hansbo, P., and Larson, M. G. Energy norm a posteriori error estimation for discontinuous Galerkin methods. *Comput. Methods Appl. Mech. Engrg. 192*, 5-6 (2003), 723–733.

[5] Beirão da Veiga, L., Niiranen, J., and Stenberg, R. A-posteriori error estimates for the Morley plate bending element. *Numer. Math. 106*, 2 (2007), 165–179.

[6] Beirão da Veiga, L., Niiranen, J., and Stenberg, R. A family of C^0 finite elements for Kirchoff plates I. Error analysis. *SIAM J. Numer. Anal. 45*, 5 (2007), 2047–2071 (electronic).

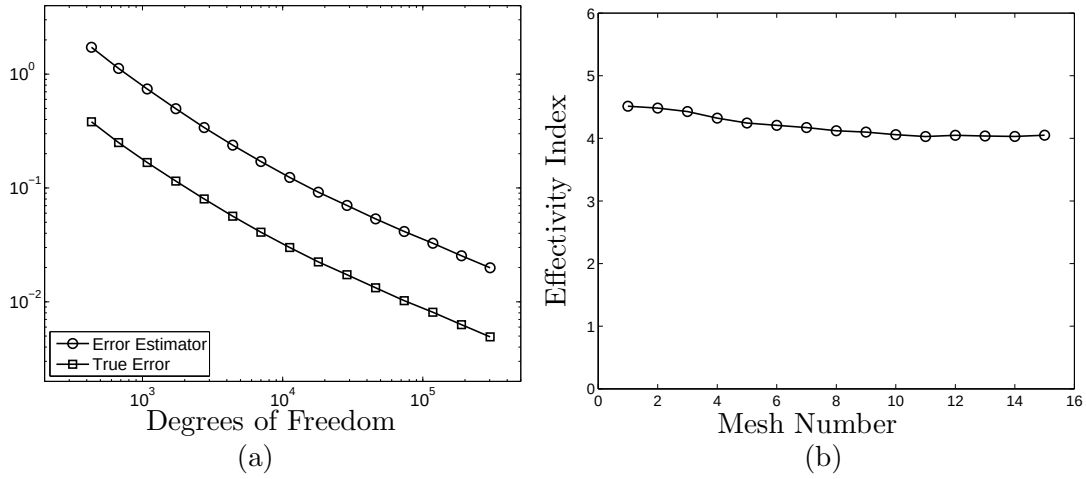

Figure 9: *Example 2.* (a) Comparison of the actual and estimated energy norm of the error with respect to the number of degrees of freedom; (b) Effectivity Indices.

[7] Brenner, S. C., and Sung, L.-Y. C^0 interior penalty methods for fourth order elliptic boundary value problems on polygonal domains. *J. Sci. Comput. 22/23* (2005), 83–118.

[8] Brezzi, F., and Fortin, M. *Mixed and hybrid finite element methods*, vol. 15 of *Springer Series in Computational Mathematics*. Springer-Verlag, New York, 1991.

[9] Carstensen, C., Gudi, T., and Jensen, M. A unifying theory of a posteriori error control for discontinuous Galerkin FEM. *submitted for publication*.

[10] Ciarlet, P. G. *The finite element method for elliptic problems*, vol. 40 of *Classics in Applied Mathematics*. Society for Industrial and Applied Mathematics (SIAM), Philadelphia, PA, 2002. Reprint of the 1978 original.

[11] Cockburn, B., Karniadakis, G. E., and Shu, C.-W., Eds. *Discontinuous Galerkin methods*, vol. 11 of *Lecture Notes in Computational Science and Engineering*. Springer-Verlag, Berlin, 2000. Theory, computation and applications, Papers from the 1st International Symposium held in Newport, RI, May 24–26, 1999.

[12] Destuynder, P., and Salaun, M. *Mathematical analysis of thin plate models*, vol. 24 of *Mathématiques & Applications (Berlin) [Mathematics & Applications]*. Springer-Verlag, Berlin, 1996.

[13] Douglas, Jr., J., Dupont, T., Percell, P., and Scott, R. A family of C^1 finite element with optimal approximation properties for various Galerkin methods for 2nd and 4th order problems. *RAIRO Anal. Numér. 13*, 3 (1979), 227–255.

[14] Engel, G., Garikipati, K., Hughes, T. J. R., Larson, M. G., Mazzei, L., and Taylor, R. L. Continuous/discontinuous finite element approximations of fourth-order elliptic problems in structural and continuum mechanics with applications to thin beams and plates, and strain gradient elasticity. *Comput. Methods Appl. Mech. Engrg. 191*, 34 (2002), 3669–3750.

[15] Eriksson, K., Estep, D., Hansbo, P., , and Johnson, C. Introduction to adaptive methods for differential equations. *Acta Numerica* (1995), 105–158.

[16] Feng, X., and Karakashian, O. A. Fully discrete dynamic mesh discontinuous Galerkin methods for the Cahn-Hilliard equation of phase transition. *Math. Comp. 76*, 259 (2007), 1093–1117 (electronic).

[17] Georgoulis, E. H., and Houston, P. Discontinuous Galerkin methods for the biharmonic problem. *IMA Journal of Numerical Analysis, to appear*.

[18] Hansbo, P., and Larson, M. G. A discontinuous Galerkin method for the plate equation. *Calcolo 39*, 1 (2002), 41–59.

[19] Hansbo, P., and Larson, M. G. A posteriori error estimates for continuous/discontinuous Galerkin approximations of the Kirchhoff-Love plate. *Chalmers University of Technology Preprtint 2008:10* (2008).

[20] Houston, P., Schötzau, D., and Wihler, T. P. Energy norm a posteriori error estimation of *hp*-adaptive discontinuous Galerkin methods for elliptic problems. *Math. Models Methods Appl. Sci. 17*, 1 (2007), 33–62.

[21] Karakashian, O. A., and Pascal, F. A posteriori error estimates for a discontinuous Galerkin approximation of second-order elliptic problems. *SIAM J. Numer. Anal. 41*, 6 (2003), 2374–2399 (electronic).

[22] Mozolevski, I., and Süli, E. A priori error analysis for the *hp*-version of the discontinuous Galerkin finite element method for the biharmonic equation. *Comput. Methods Appl. Math. 3*, 4 (2003), 596–607 (electronic).

[23] Mozolevski, I., Süli, E., and Bösing, P. *hp*-version a priori error analysis of interior penalty discontinuous Galerkin finite element approximations to the biharmonic equation. *J. Sci. Comput. 30*, 3 (2007), 465–491.

[24] Neittaanmäki, P., and Repin, S. A posteriori error estimates for boundary-value problems related to the biharmonic operator. *East-West J.Numer. Math. 2* (2001), 157–178.

[25] Süli, E., and Mozolevski, I. *hp*-version interior penalty DGFEMs for the biharmonic equation. *Comput. Methods Appl. Mech. Engrg. 196*, 13-16 (2007), 1851–1863.

[26] Verfürth, R. *A Review of* A Posteriori *Error Estimation and Adaptive Mesh-Refinement Techniques*. Wiley-Teubner, Chichester-Stuttgart, 1996.

List of Figures